

## The effect of porphyrin supramolecular structure on singlet oxygen photogeneration

A. Solovieva<sup>a,\*</sup>, G. Vstovsky<sup>a</sup>, S. Kotova<sup>a</sup>, N. Glagolev<sup>a</sup>, B.S. Zav'yalov<sup>b</sup>, V. Belyaev<sup>a</sup>, N. Erina<sup>c</sup>, P. Timashev<sup>b</sup>

<sup>a</sup>*N.N. Semenov Institute of Chemical Physics of Russian Academy of Sciences, Polymer Department, 4, Kosygin St., Moscow, 119991, Russia*

<sup>b</sup>*L. Ya. Karpov Institute of Physical Chemistry, Vorontsovo Pole, 10, Moscow, 103064 Russia*

<sup>c</sup>*Veeco Metrology Group, 112 Robin Hill Road, Santa Barbara, CA 93117, USA*

Received 20 April 2005; revised 6 May 2005; accepted 8 May 2005

### Abstract

This work is to show that activity of porphyrins in singlet oxygen generation (SOG) is determined not only by their molecular structure but also by supramolecular structure of porphyrin containing systems. This is demonstrated by results of studies of SOG in the gas phase by vacuum deposited tetraphenylporphyrin (TPP) layers under photoexcitation conditions. The structure of the layers was studied by atomic force microscopy (AFM), TEM in diffraction regime (TED) and by the flicker-noise spectroscopy (FNS) method. It was shown that substrates affect the deposited layers structure only at earlier stages of the layer formation. AFM and TED data, together with FNS quantitative parameters of TPP layers, show directly that the chemical activity of solid-phase systems can be determined not only by their chemical nature but also by their supramolecular structure.

© 2005 Elsevier Ltd. All rights reserved.

**Keywords:** AFM; TED; Porphyrin; Singlet oxygen generation; Supramolecular structure

### 1. Introduction

From a most general viewpoint, the structure of porphyrin layers obtained by vacuum deposition or precipitation from solution must be determined by both the structure of their molecules and by their ability to form aggregates during layer formation, due to the intermolecular interactions that are responsible for a supramolecular structure (Solovieva and Timashev, 2003; Kunitake et al., 1995; Hiruma and Hamamatsu, 2002; Labardi et al., 1994; Grafstrom et al., 1990). Thus to study such systems adequately, instead of a scheme like ‘molecular structure–chemical activity’, we must consider a triad: ‘molecular structure–supramolecular structure–chemical activity’.

The process of singlet oxygen  ${}^1\text{O}_2$  generation (SOG) has been attracting much attention recently because of its potential ability to initiate reactions of sensitized oxidation

of biologically active compounds and in the photodynamic therapy of cancer. The deposited porphyrin layers were found to be active in providing SOG into the gas phase under photosensitized excitation of adsorbed molecular oxygen  ${}^3\text{O}_2$  (Solovieva and Timashev, 2003). Such systems are interesting as the models to be studied before investigation of really complex systems.

The problem arises: how can the features of deposited layers be evaluated quantitatively and related to their chemical activity? This work proposes a possible solution of the problem for the case of gas-phase SOG by vacuum deposited tetraphenylporphyrin (TPP) layers (VDTPPL) (both island and continuous films) under photoexcitation conditions. For this goal, atomic force microscopy (AFM) and transmission electron microscopy diffraction (TED) are the appropriate experimental techniques that allow us to study surface structures appearing at the mcm and nm scales (see Wada et al., 2000; Collier et al., 1999; Lopinski et al., 2000; Siegenthaler, 1992; Srinivasan et al., 1991; Tao and Shi, 1994; Yaminsky and Elensky, 1997; Yokoyama et al., 2001). For example, we can study the (poly)crystalline structure of TPP aggregates (Solovieva and Timashev,

\* Tel.: +095 939 7395; fax: +095 137 8284.

E-mail address: anna@polymer.chph.ras.ru (A. Solovieva).

2003) and the effect of substrates on VDTPPL structure. For quantitative VDTPPL structure analysis we have used flicker–noise spectroscopy (FNS) (Solovieva et al., 2003; Vstovsky et al., 2001; Timashev and Vstovsky, 2003; Timashev et al., 2003; Timashev, 2000; Timashev, 2001).

The structure of VDTPPL was studied in the range of the TPP surface concentration given by  $N_{\text{tot}} \sim 10^{-11}$ – $10^{-9}$  mol/cm<sup>2</sup>. The rate of  $^1\text{O}_2$  generation was shown to be dependent on the structural parameters of the deposited layers on a scale of up to some fractions of a micrometer. Formation of VDTPPL is due to Van-der-Waals interaction between TPP molecules and TPP molecules with the substrates.

## 2. Experimental results

The dependencies of SOG efficiency (the rate and quantum yield of generation) on the total TPP surface concentration are shown in Fig. 1, for the case of TPP deposited on quartz. A detailed description of experimental measurements is given in Appendix A (Solovieva et al., 2000; Turro et al., 1981). The SOG rate has a maximum in the concentration range  $N_{\text{tot}} \sim (4\text{--}12) \times 10^{-11}$  mol/cm<sup>2</sup>, while the quantum yield decreases with increase in TPP surface concentration. The formal kinetic scheme of SOG (Solovieva et al., 2000; Turro et al., 1981; Neckers, 1967) given in Appendix B shows that although it includes all the relevant SOG processes, the resulting formula (2.5) describes saturation but cannot describe the drop of the experimentally observed dependence  $C_S = C_S(N_{\text{tot}})$ . This observation may be due to dependence of the constants  $k_1$ ,  $k_2$ ,  $k_3$  and  $k_4$  on the total concentration of TPP molecules taking part in photosensitized SOG. These dependences can be due to structural effects of TPP (nano- and micrometer) aggregates, i.e. supramolecular structure. To investigate the features of this structure, our AFM and TED investigations were carried out.

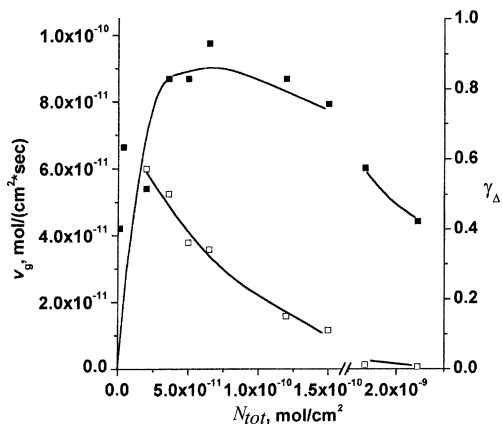


Fig. 1. The rate (■) and quantum yield (□) of singlet oxygen generation by TPP for different surface concentrations.

TED investigations were necessary to establish the crystalline structure of TPP aggregates on the substrate surface. But because they require the rather small NaCl substrates ( $< 1 \times 1 \text{ cm}^2$ ) with area not large enough to study SOG efficiency (see Appendix A; quartz substrates were used), the effects of various substrates on VDTPPL structure must be investigated additionally to compare correctly the parameters of VDTPPL structure and their SOG activity.

For TED observations, carbon was deposited on NaCl substrates with TPP (for TPP deposition, see Appendix A); then NaCl samples with deposited porphyrin and carbon were dissolved in water and carbon replicas (with porphyrin attached) were studied using by a JEM-2000EX microscope over a period of 3–10 min with an electron energy of 200 keV. For AFM, TPP was deposited on quartz and mica substrates and, the samples were studied using a Solver-P47 AFM (NT-MDT, Zelenograd, Moscow region) in tapping mode.

The experiments on mica and quartz showed that the formation of layers starts with small aggregates (islands) for  $N_{\text{tot}} \sim 10^{-12}$ – $10^{-11}$  mol/cm<sup>2</sup>. The average peak height was 30–40 nm for mica and 50–60 nm for quartz substrates (Fig. 2). As the TPP surface concentration increased, the number and size of the aggregates grew.

When the surface concentration reached 1.5–2.0  $10^{-9}$  mol/cm<sup>2</sup> for mica and about  $10^{-10}$  mol/cm<sup>2</sup> for quartz, the growth of individual aggregates almost stopped and a continuous layer was formed (Fig. 3). The sizes of largest individual aggregates reached 150–200 nm in height and 1–3  $\mu\text{m}$  in diameter, both for mica and quartz substrates (Fig. 4). Thus the maximum sizes of individual islands and the configuration of continuous layers were similar for both quartz and mica. However, the formation of the continuous film on quartz took place at lower concentrations, probably because of its higher irregularity (Fig. 5). (The AFM patterns are smaller than  $20 \times 20 \mu\text{m}$  to show the difference in smoothness of the surfaces.)

TED allowed us to obtain electron diffraction patterns suitable for the determination of the averaged crystalline structure of individual TPP aggregates (Fig. 6). For small  $N_{\text{tot}}$ , the deposited layer consists predominantly of small ‘islands’. These islands had a crystalline structure. When the deposited layer became continuous, its diffraction pattern was characteristic of a polycrystalline phase. This implies that the NaCl monocrystalline substrate might affect the orientation of small porphyrin crystals at the initial stages of deposited layer formation but it had no effect when the layer became continuous.

In accordance with the AFM and TED data, the nature and surface structure of the support influenced only the initial stages of the VDTPPL formation. However, the structure of a continuous deposited TPP film was not influenced by the substrate surface.

This conclusion was confirmed by a calculation of the surface area of deposited TPP. The area was calculated by triangulation of digital patterns. The description of

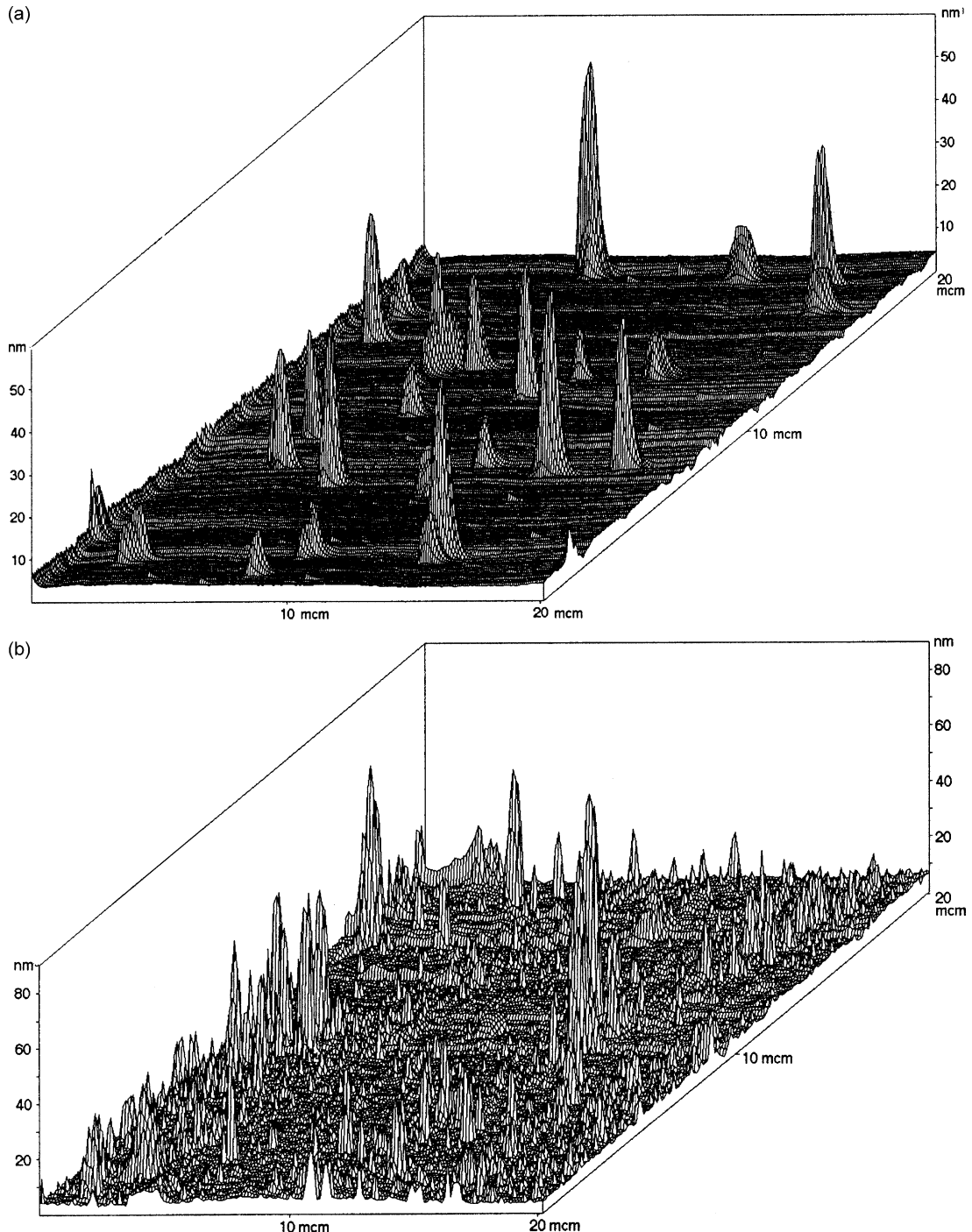


Fig. 2. AFM patterns of TPP deposited on mica (a) and quartz (b).

the area calculation is given in detail in Appendix C. Results of that calculation for  $20 \times 20 \mu\text{m}$  ( $4.0 \times 10^{-10} \text{ m}^2$ ) fragments are given in Fig. 7. The maximum value of the surface fragment area was approximately  $4.2 \times 10^{-10} \text{ m}^2$  for both the mica and quartz cases, when continuous TPP deposited layers had been formed. This value is determined by the overall surface roughness. For continuous films, increase in the TPP surface concentration did not change the surface area.

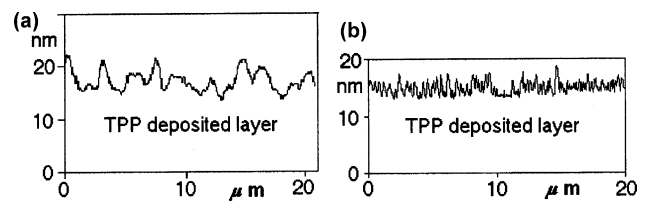


Fig. 3. Typical AFM patterns sections of continuous TPP deposited layer on mica (a) and quartz (b).

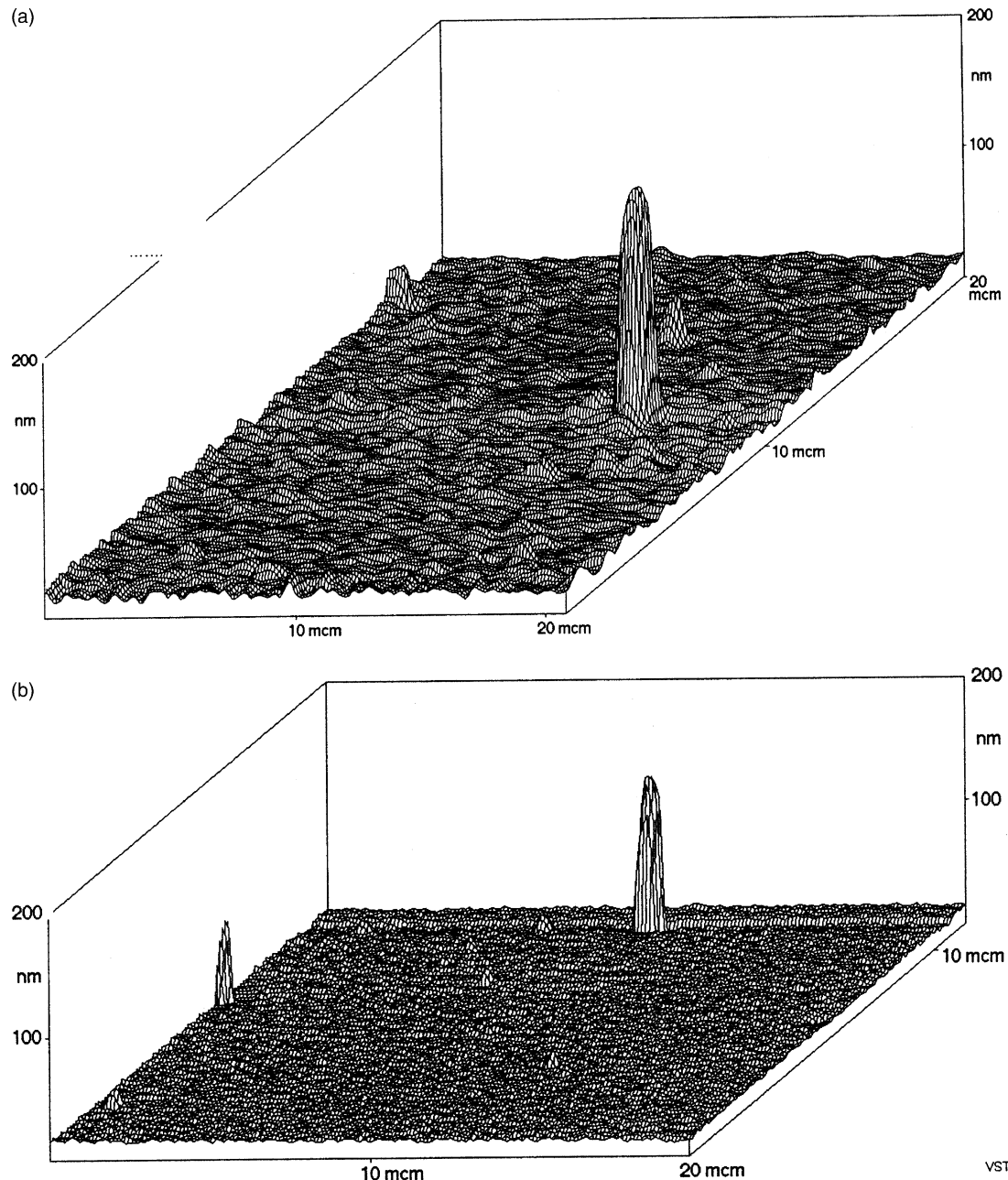


Fig. 4. Typical AFM patterns of TPP deposited on mica ( $N_{\text{tot}} = 1.3 \times 10^{-9} \text{ mol/cm}^2$ ) (a) and quartz ( $N_{\text{tot}} = 2.4 \times 10^{-10} \text{ mol/cm}^2$ ) (b).

The AFM data were also processed with a special program implementing the flicker-noise spectroscopy (FNS) method. This method was developed recently for the analysis of chaotic structures and for obtaining the sets of parameters of surface structures (Vstovsky et al., 2001; Timashev and Vstovsky, 2003; Timashev et al., 2003). The results of our analysis are given in Table 1. For the quantitative description of surface structures, the following parameters were used: the average height of surface roughness  $h$ , corresponding standard deviation  $\sigma$ , correlation lengths  $L_0$  and  $L_1$ , assigned to the major types of surface irregularities—the ‘spikes’ and ‘jumps’, respectively, according to a general FNS concept (Timashev, 2000;

Timashev and Vstovsky, 2003) and also the dimensionless parameters  $n$  and  $H$  (the Hurst parameter). Calculation technique of these parameters is given in Appendix D. The correlation lengths describe a ‘memory’ in the sequences of ‘spikes’ and ‘jumps’ that form the surface roughness according to general FNS concept, while  $n$  and  $H$  describe the extent of the correlation loss in these sequences. In general, the totality of these parameters shows the degree of surface ‘organization’.

A definite surface disordering with growth of the TPP surface concentration was observed. It was manifested by a decrease in the correlation lengths  $L_1$  and  $L_0$  and also by increase in the value of  $n$  (Table 1) that probably indicates

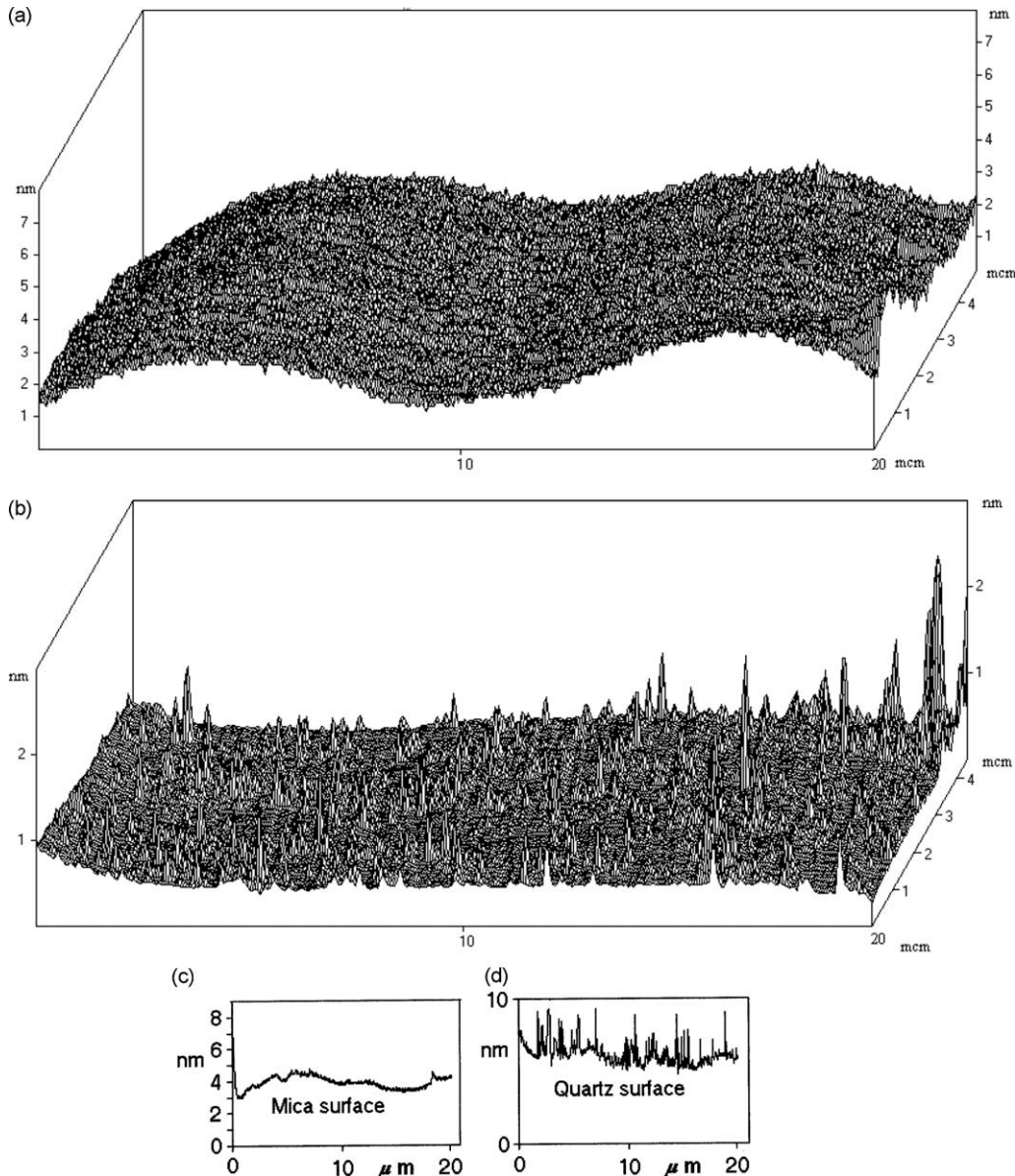


Fig. 5. Typical AFM patterns of clean mica (a) and quartz (b) substrates and some of their sections (c) and (d), respectively.

chaotic growth of the deposited layers surface. It is important to note that the  $L_1$  and  $L_0$  values for the continuous TPP layers are close to those for mica and quartz. The main feature of the data in Table 1 is that the parameters  $n$ ,  $L_0$  and  $L_1$  are close in value for continuous layers, both on mica and on quartz (the fourth lines in the ‘Mica’ and ‘Quartz’ sections). This means that the properties of the deposited layers are determined by the properties of the support surface, for earlier stages of the VDTPPL formation only.

On the whole, the effects of the support (mica, quartz or NaCl) seemed to be essential only at the initial stages of formation of the deposited layer (for the low TPP surface concentrations). At the same time, the structure of continuous porphyrin layers on nano- and microscales is

determined mostly by intermolecular interactions of porphyrin molecules and their aggregates.

### 3. Discussion

As seen from the described results, decrease in the correlation lengths ( $L_0$  in about 2 times and  $L_1$  in about 5 times, Table 1) of VDTPPL on quartz substrates corresponds to a decrease in SOG efficiency: for a 2-fold increase in TPP surface concentration,  $N_{\text{tot}}$  grows in the range  $10^{-10}$ – $10^{-9}$  mol/cm<sup>2</sup> (Fig. 1), for a continuous film on quartz. The corresponding characteristic sizes (evaluated by  $L_1$ ) of the correlated regions (inside which the surface can be considered as homogeneous) change approximately

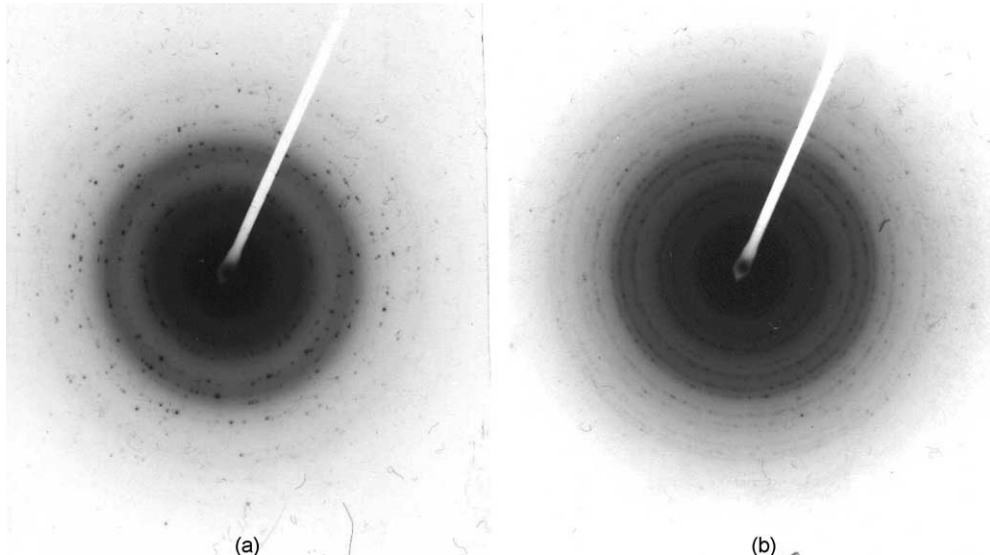


Fig. 6. The diffraction patterns of a deposited TPP layer consisting of ‘islands’ ( $N_{\text{tot}}=4\times 10^{-11} \text{ mol/cm}^2$ ) (a) and of a continuous layer ( $N_{\text{tot}}=8\times 10^{-9} \text{ mol/cm}^2$ ) (b).

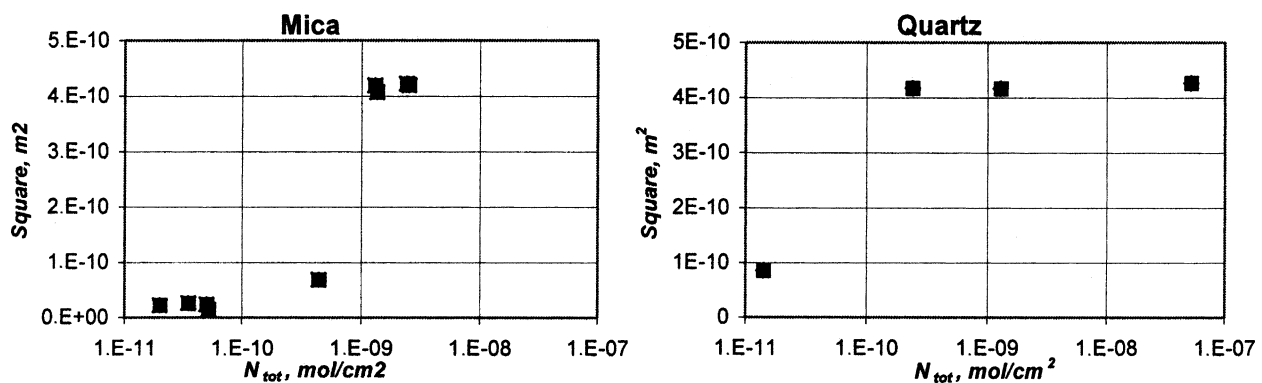


Fig. 7. Results of TPP deposited layers surface calculation for pieces  $20\times 20 \mu\text{m}^2$  ( $4\times 10^{-10} \text{ m}^2$ ).

from 500 to 100 nm. Surface fragments of greater length are heterogeneous. From a general viewpoint (Solovieva and Timashev, 2003), effects of VDTPL surface organization on surface chemical activity are due to inevitable processes of chemosorption of molecular oxygen and desorption of singlet oxygen, both being influenced by

surface-structural rearrangements. Thus the disordering of the VDTPL surface is followed by decrease in SOG efficiency that points to a role of surface organization over a length scale up to fractions of a micrometer, i.e. the supramolecular structure, responsible for VDTPL chemical activity.

Table 1  
The Flicker-noise spectroscopy parameters of the deposited TPP layers (Solver-P47, NT-MDT)

$N_{\text{tot}}$ , mol/cm <sup>2</sup>	$n$	$L_0$ , $\mu\text{m}$	H	$L_1$ , $\mu\text{m}$	$h$ , $\mu\text{m}$	$\sigma$ , $\mu\text{m}$
<b>Mica</b>						
$2.00 \times 10^{-11}$	1.76	0.67	0.87	0.51	0.014	0.0015
$3.50 \times 10^{-11}$	1.93	0.77	0.92	0.43	0.024	0.0032
$1.30 \times 10^{-9}$	2.73	0.75	0.97	0.29	0.022	0.0053
$2.40 \times 10^{-9}$	4.50	0.34	0.90	0.10	0.032	0.0111
<b>Quartz</b>						
$1.40 \times 10^{-11}$	4.78	0.65	0.70	0.60	0.008	0.0022
$2.39 \times 10^{-10}$	4.35	0.46	0.57	0.44	0.026	0.0021
$1.28 \times 10^{-9}$	5.11	0.32	0.68	0.20	0.012	0.0027
$5.15 \times 10^{-8}$	5.05	0.27	0.61	0.08	0.019	0.0042

Each value was calculated by averaging over 3–8 surface fragments of  $20\times 20 \mu\text{m}$  ( $1000\times 1000$  points for mica samples and  $1024\times 1024$  for quartz samples).

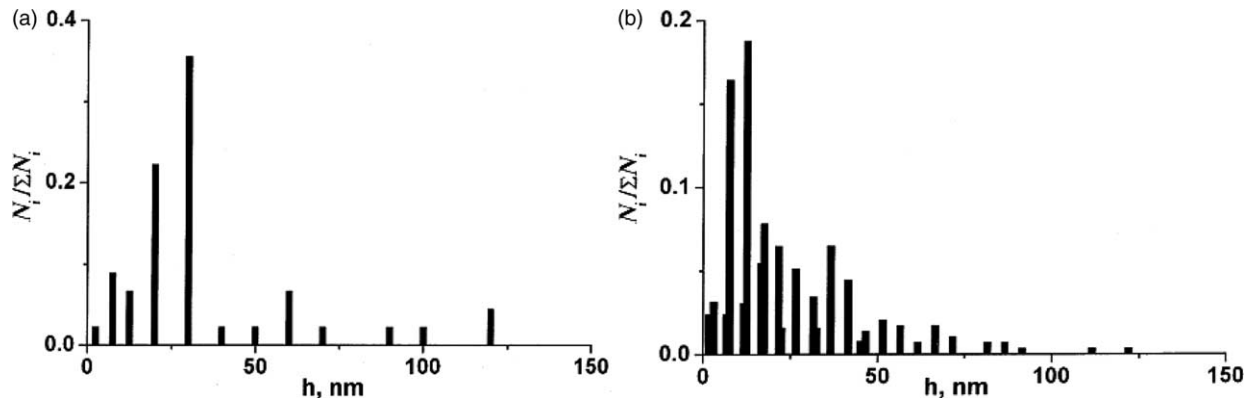


Fig. 8. The height distribution of TPP ‘islands’ on the mica surface according to the AFM data:  $N_{\text{tot}} = 1.5 \times 10^{-12} \text{ mol/cm}^2$  (a),  $N_{\text{tot}} = 3.6 \times 10^{-11} \text{ mol/cm}^2$  (b).

This conclusion about the role of surface heterogeneity, on the scales of a fraction of a mcm is consistent with literature data. For example: (i) According to the results of a scanning tunneling microscopy (STM) investigation (Zambelli et al., 1997), the dissociative adsorption of molecular oxygen on platinum introduces intense rearrangement of the Pt surface structure at spatial scale of the order of a micrometer. (ii) As was shown in Mitsui et al. (2003), dissociative hydrogen adsorption on palladium requires three or more vacancies and requires correlated surface excitation on the same spatial scale. (This result was obtained by the STM observations of the transient formation of active sites for the dissociative adsorption of H<sub>2</sub> on the Pd (111) surface.) (iii) The data on the behavior of lead particles with nano-crystal sizes (4–10 nm) obtained by high resolution electron microscopy also indicate the possibility of dynamic rearrangements of solid fragments in the same surface scale range (Ben-David et al., 1997). Thus we have confirmed a general conclusion, discussed in Solovieva and Timashev (2003), about the role of surface heterogeneity in heterogeneous catalysis.

As to our VDTPPL study, in accordance with the results described, the structural features of the porphyrin layers on the submicrometer scales influence the rate of <sup>1</sup>O<sub>2</sub> generation under permanent photoexcitation of these layers. Indeed, the very features of the structure of porphyrin surface layers (detected by the FNS-based analysis of the AFM data) determine the process of electron-vibrational excitation transfer in the surface porphyrin layers (Solovieva and Timashev, 2003). In particular, it may be assumed that the decrease in the correlation degree of the crystal structure fragments of the surface layers (described by the drop of  $L_1$  and by the growth of  $n$ ) results in the decrease of the apparent constants  $k_1$  and  $k_2$  and in the increase of constant  $k_3$ ; see Appendix B. Of course, the active sites, where <sup>1</sup>O<sub>2</sub> surface desorption occurs, can be related to some local structural irregularities on an atomic scale. However, the rate of energy accumulation at these sites (enough to inject singlet oxygen into the gas phase) due to surface-fragment rearrangement under continuous

photoexcitation can depend on the structural state of the surface on the submicrometer scale reflected by FNS parameters. So the point is that, although a single act of excitation transfer from excited porphyrin molecule to the oxygen takes place on an atomic scale, the ‘gross’ SOG effect is determined by the ability of the singlet oxygen to escape from the surface and that in turn is determined by the surface structure on a submicrometer scale.

Analysis of AFM-images of deposited TPP layers surfaces shows that their patterns change as the deposited porphyrin concentration grows. Their roughness increases and this results in growth of the total area of the deposited layer surface (Fig. 7). At the same time, the average height of ‘islands’ does not change significantly with the growth of the surface concentration; rather small (lower than 50 nm) ‘islands’ dominate at any concentration (Fig. 8). The decrease in the efficiency of singlet oxygen generation with the growth of the porphyrin surface concentration

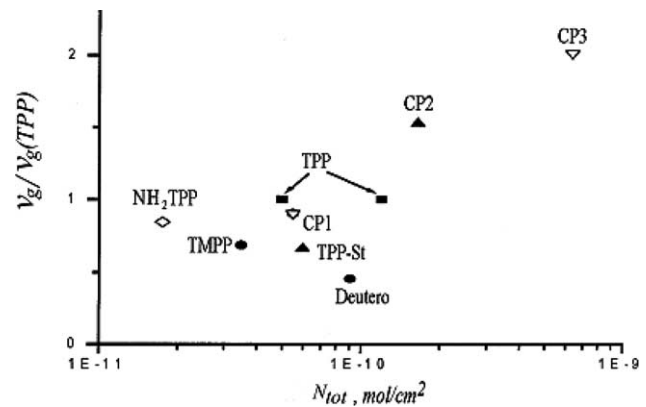


Fig. 9. A comparative diagram of singlet oxygen generation efficiency by different porphyrins. (The efficiency of generation for TPP is accepted as 1.) TPP, meso-tetraphenylporphyrin, TMPP, meso-tetra(*p*-methoxyphenyl)porphyrin, NH<sub>2</sub>TPP, meso-( $\alpha$ -*p*-monoaminophenyl,  $\beta,\gamma,\delta$ , triphenyl)porphyrin, TPP-St, ( $\alpha$ -*p*-stearoylamidophenyl,  $\beta,\gamma,\delta$ -triphenyl)porphyrin, Deutero, dimethyl ether of deuteroporphyrin, CP<sub>1</sub>, 1,3,5,8-tetramethyl-2,4-divinyl-6,7[2'benzyloxy carbonyl]ethyl-(7(6)-2'-(*m*-carboran-9-yl)oxycarbonyl]ethylporphyrin, CP<sub>2</sub>, 1,3,5,8-tetramethyl-6,7-di-[2*N*-(*o*-carboran-3-yl)carbamoylethyl]porphyrin, CP<sub>3</sub>, 1,3,5,8-tetramethyl-6,7-di[(2-*m*-carboran-9-yl)methoxycarbonylethyl] porphyrin.

means that the generation process is determined by the supramolecular structure. This implies that the dynamics of redistribution and ‘concentration’ of the excitation energy in the polymolecular layers plays a major role in the formation of local dynamical fluctuations, which are sufficient to inject singlet oxygen molecules into the gas medium.

Correlation of FNS parameters with the surface concentration (Table 1), reflecting quantitatively the degree of chaos in a deposited layer, corresponds ultimately to the tendency of the singlet oxygen generation rate to decrease. It should be pointed out that this result is not trivial: under the conditions of photoexcitation of the deposited TPP layers studied here, the rate of singlet oxygen generation is determined by the structure peculiarities of such layers on scales that exceed the atomic scale (fractions of a nanometer) by two orders of magnitude.

#### 4. Conclusions

In conclusion, it should be pointed out that the processes of sensitized SOG under photoexcitation of the deposited layers appear to be dependent on the chemical structure of other porphyrin molecules but this dependence is not ‘direct’ or ‘immediate’. This is demonstrated in Fig. 9, where data on the steady-state singlet oxygen concentration in the gas phase are shown for the deposited layers of various porphyrins under the same experimental conditions, for surface concentrations  $N_{\text{tot}} = 10^{-11} - 10^{-9} \text{ mol/cm}^2$ . The values of steady-state concentration are normalized by the maximum observed value TPP singlet-oxygen concentration. As follows from Fig. 9, the difference in the singlet oxygen generation efficiency can vary by half an order of magnitude. For example, deuteroporphyrin is characterized by the lowest efficiency while deuteroporphyrins containing carboranyl substituents ( $CP_2$  or  $CP_3$ ) have the highest efficiency. In solutions or in an immobilized state, these porphyrins have almost a unity quantum yield of SOG (Solovieva and Timashev, 2003). The  $CP_2$  or  $CP_3$  molecules possess bulky substituents, unlike the plane molecules of non-substituted deuteroporphyrin which have very dense packing in the deposited layer (as well as in any aggregates). These data directly show that chemical activity of solid-phase porphyrin containing systems is determined not only by their chemical nature but also by their supramolecular structure.

#### 5. Appendices

##### A. Investigation of singlet oxygen generation

The process of singlet  ${}^1O_2$  oxygen photogeneration into the gas phase was investigated under the photoexcitation of polymolecular layers of TPP and other porphyrin photosensitizers (PPS). Porphyrins were deposited onto  $20 \text{ cm}^2$

quartz plates using a VUP-4 vacuum evaporation unit at a residual pressure  $10^{-4}$  Torr and evaporation rate  $\approx 3.1 \times 10^{-12} \text{ mol}/(\text{cm}^2 \times \text{sec})$  at  $300^\circ\text{C}$ . The temperature of the quartz plates was about  $20^\circ\text{C}$  and did not change significantly during the time (5–10 min) of deposition. The substrate surface was at first ground according to the 14th purity class and then annealed in the flame of a Bunsen burner. The porphyrin surface concentration was determined on the basis of the intensity of the Soret band in the electron spectra of porphyrin solutions in chloroform, obtained by washing the deposited layers after all the measurements were done. The lowest measurable concentration was  $1.5 \times 10^{-12} \text{ mol}/\text{cm}^2$  and this value was taken as an accuracy of the surface concentration measurements. The overall range of the studied PPS surface concentrations was  $10^{-12} - 10^{-8} \text{ mol}/\text{cm}^2$ .

The efficiency of singlet oxygen generation was investigated in an all-soldered glass unit filled with molecular oxygen with the quartz plate inside. The working pressure of molecular oxygen was 13 Pa. The generated singlet oxygen was detected by a semiconductor (ZnO) sensor. The rate  $v_g$  of  ${}^1O_2$  generation was measured based on the steady-state  ${}^1O_2$  concentration  $C_{\text{st}} = v_g/K_q$  (where  $K_q$  is a term representing the rates of all the processes of singlet oxygen quenching inside the experimental unit) under continuous photoexcitation of the system (Solovieva et al., 2000). A mercury lamp DRSh-500 with a light filter BS-8 and a water filter (the total transmission band is 350–1000 nm) was used as the light source. No singlet oxygen generation was registered in the absence of a porphyrin on the quartz plate. The ZnO sensor was calibrated by measuring a singlet oxygen signal from a controllable source of  ${}^1O_2$ . 9,10-Diphenylanthracene endoperoxide (DPAE) was used as the source. If heated, it decomposed and gave equimolar quantities of  ${}^1O_2$  and 9,10-diphenylanthracene (DPA) (Turro et al., 1981). The quantity of the DPA obtained was measured from its electron absorption spectrum, and thus the rate of singlet oxygen generation was calculated. DPAE was synthesized from DPA by photochemical oxidation (Turro et al., 1981).

The structure of the deposited polymolecular porphyrin layers was determined using transmission electron microscopy (TEM) and atomic force microscopy (AFM).

The corresponding samples were prepared by the simultaneous depositions of porphyrins onto quartz plates (for the investigation of SOG and for AFM), onto monocrystalline NaCl plates (for TEM) and onto mica plates (for AFM). An NaCl sample with the deposited porphyrin after covering with carbon was put into water. Then the carbon replica with porphyrin was studied using a transmission electron microscope. The electron energy was 200 keV, the duration of electron irradiation was 3–10 min. The mica plates (having a smoother surface) were used to show to what extent the structure of the deposited layers was determined by the support surface smoothness.

The TEM data were obtained with a JEM-2000 EX-II microscope. The AFM investigations were carried out using a Solver-P47 microscope (NT-MDT, Zelenograd, Moscow region) in the tapping mode. The electron absorption spectra were obtained using a Specord UV-VIS spectrophotometer.

### B. Formal kinetics of SOG

The process of photosensitized generation of singlet oxygen starts with excitation of a sensitizer molecule and includes several stages (Solovieva et al., 2000; Neckers, 1967). After absorption of photons, porphyrin molecules in their singlet ground state  $^1P$  transfer into the excited state  $^1P^*$ . Porphyrin molecules in the triplet state  $^3P^*$  are generated by the processes of intercombination conversion in the porphyrin molecular crystal fragments, due to the corresponding electron-vibrational transitions. Coordination of oxygen molecules in the ground triplet state  $^3O_2$  near porphyrin molecules in the excited triplet state  $^3P^*$  results in the excitation energy transfer to molecular oxygen. Oxygen molecules in the singlet excited state  $^1O_2$  are also coordinated near porphyrin molecules. The latter means that  $^1O_2$  generation is possible only if the characteristic desorption time for singlet oxygen molecules is shorter than the time of their deactivation in the coordinated state. Below we have eliminated some of the described intermediate stages for the purposes of qualitative analysis of these processes in the framework of a formal kinetic scheme. Thus the process of photosensitized SOG into gas phase due to absorption of a light quantum  $h\nu$  is presented by the following scheme



Here  $k_1$ ,  $k_2$ ,  $k_3$  and  $k_4$  are the corresponding rate constants of the described processes (I–IV): appearance of porphyrin molecules in the triplet spin state  $^3P^*$ ,  ${}^1O_2$  molecules generation into gas phase, deactivation of the porphyrin  ${}^3P^*$  state, deactivation of  ${}^1O_2$  molecules on the walls and in the volume of an experimental unit. It is clear a priori that transformations I–III of this scheme take place on the surface of a porphyrin layer and the corresponding rates must be determined by the surface concentrations of the reactants. All the constants included in the set of equations given below are adopted as effective ones. Since the equilibrium between adsorbed and gas-phase oxygen molecules is established rapidly enough, the corresponding equations of formal chemical kinetics for the concentrations

$C_S$  and  $C_T$  of oxygen molecules in singlet and triplet states in gas phase are as follows.

$$\frac{dN^*}{dt} = k_1 w N - k_2 C_T N^* - K_3 N^* = 0, \quad (2.1)$$

$$\frac{dC_s}{dt} = k_2 C_T N^* - k_4 C_s = 0, \quad (2.2)$$

$$N_0 = N + N^*, \quad (2.3)$$

$$C_0 = C_T + C_s. \quad (2.4)$$

Here  $w$  is a parameter characterizing the energy absorption by a deposited layer under photoexcitation (determined by the porphyrin extinction and the effective thickness of the absorbing layer);  $N$  and  $N^*$  are the surface concentrations of  $^1P$  and  ${}^3P^*$  porphyrin molecules taking part in photogeneration of singlet oxygen;  $N_0$  is the total concentration of TPP molecules taking part in photosensitized generation of singlet oxygen, and  $C_0$  is the total oxygen concentration in gas phase.

The solution of the system for the steady-state concentration  $C_S$  of singlet oxygen in gas phase reads

$$C_S(N_0) = \frac{k_1 k_2 w N_0 C_0}{k_3 k_4 + k_1 w (k_4 + k_2 N_0) + k_2 k_4 C_0} \quad (2.5)$$

Note that Eq. (2.5) describes saturation but does not describe the drop in the experimentally observed dependence  $C_S = C_S(N_{\text{tot}})$ . This fact may be related to a dependence of the constants  $k_1$ ,  $k_2$ ,  $k_3$  and  $k_4$  on  $N_0$ . It should be pointed out that, assuming  $N_0 = \theta N_{\text{tot}}$ , where  $\theta$  is the fraction of porphyrin molecules taking part in the photosensitization processes, introduction of any form of dependence  $\theta(N_{\text{tot}})$  cannot provide a description of the drop of  $C_S(N_{\text{tot}})$  dependence for higher TPP surface concentrations.

### C. Calculation of surface-fragment area

The area of an elementary surface fragment for each four neighboring heights A, B, C, D can be calculated as a sum of two triangles: ABD and BCD, or ABC and ACD, and was taken as a mean of these two sums. The overall area of a surface fragment can be calculated as a sum over all the four of the heights. For the patterns of discontinuous TPP layers (island films), an additional procedure was applied before the surface calculation. First, for each pattern the overall range of heights was partitioned into 50 subranges, and the subrange containing the maximum number of points was set as the ‘zero’ z-level which was assumed to correspond to the support surface. The area was calculated by a special program for such pattern regions that are higher than the ‘zero’ level.

#### D. Flicker noise spectroscopy based on AFM data processing

Usually the SPM-based analysis of surface structure uses processing of digitized ‘roughness profiles’ obtained by scanning a studied surface fragment with the characteristic sizes from several nanometers to tens of micrometers. As a rule, the results are presented in the form of images of individual surface structure fragments (for example, molecular aggregates) or the images of general surface morphology under the conditions of ‘model lighting’ (Kunitake et al., 1995; Hiruma and Hamamatsu, 2002; Labardi et al., 1994; Grafstrom et al., 1990). In order to obtain high quality images and to decorate the molecular aggregates and supramolecular structures of polymers (spherulites, lamellae and other structural elements) a primary surface treatment is usually used (e.g. etching). These images may greatly depend on the localization of the model lighting, and very different images of the same surface fragment might result from different sources of light.

In general, there exists no standard and conventional method of digitized data processing that allow calculation of cumulative parameters characterizing the features of the studied surface as a whole. The purely statistical processing methods, which give the mean roughness values with the corresponding dispersion and cumulants, have hardly any practical value since they do not provide information about a very important property of the real structures that are self-correlated at various spatial scales. Flicker noise spectroscopy (FNS) (Solovieva et al., 2003; Vstovsky et al., 2001; Timashev and Vstovsky, 2003; Timashev et al., 2003; Timashev, 2000; Timashev, 2001) provides new opportunities for the quantitative description of real chaotic surfaces since it leans upon the information about the real structure irregularities on different length scales. The main parameters of FNS methodology are introduced below.

The FNS method, with reference to handling the temporal and spatial series (in the form of digitized sequences of numbers with an equal pitch on temporal or spatial coordinate), consists in the evaluation of the so-called structural functions (difference moments) and Fourier power spectra, which are then parameterized on the basis of nonlinear trends (parametrically specified curves). The Fourier-spectra were calculated as usual with reference to surfaces profiles with a zero medial  $\langle h'(x,y) \rangle = 0$ ,  $h'(x,y) = h(x,y) - \langle h(x,y) \rangle$ , where  $h(x,y)$  is the reference altitude of a profile. For example, for a profile, specified discretely in heights  $h'_i$  at the points  $x_i = i\Delta x$  ( $\Delta x$  is the sampling pitch) along the coordinate  $x$ , the power spectra were calculated by the formulae

$$S(k) = U^2(k) + V^2(k) \quad (4.1)$$

$$U(k) = \frac{1}{N} \sum_{i=0}^{N-1} h'_i \cos(x_{i+1} 2\pi k),$$

$$V(k) = \frac{1}{N} \sum_{i=0}^{N-1} h'_i \sin(x_{i+1} 2\pi k),$$

where the magnitude of the wave vector  $k$  varies within the limits  $[1/(N\Delta x), 1/(2\Delta x)]$  (50% of all the harmonics available),  $N = 1024$  – number of points.

In references Solovieva et al., 2003, Vstovsky et al., 2001, Timashev and Vstovsky, 2003, Timashev et al., 2003, Timashev, 2000 and Timashev, 2001, it is proposed to approximate the power spectrum by the model

$$S(k) = \frac{S_0}{1 + (L_0 \cdot k)^n} + D_0. \quad (4.2)$$

The  $S_0$ ,  $L_0$ ,  $n$ ,  $D_0$  parameters are calculated using a special algorithm for the same values of maximum and minimum  $k$  harmonics for all the profiles processed (see below). The automatic choice of the parameters of this model (for external evidence of the parameters fitted) is a nontrivial problem. The fitting algorithm needed evaluation of the  $D_0$  minimum value and then 85% of harmonics (instead of the valid 50% of available harmonics according to the Kotelnikov theorem) were calculated for this purpose.

The difference moment of the order  $p$  is

$$\Phi_{(p)}(\Delta) = \langle |h(x) - h(x + \Delta)|^p \rangle \quad (4.3)$$

(the brackets mean an average, immediate, over all the  $h(x)$  series), following references Timashev et al., 2003, Timashev, 2000 and Timashev, 2001, is approximated by the formulae

$$\Phi_{(p)}(\Delta) \approx G_1(p) \cdot \sigma^p \cdot [1 - \Gamma(H, \Delta/L_1)/\Gamma(H)]^p \quad (4.4)$$

or

$$\Phi_{(p)}(\Delta) \approx G_1(p) \cdot \sigma^p \cdot [\gamma(H, \Delta/L_1)/\Gamma(H)]^p. \quad (4.5)$$

Here  $G_1(p)$  is a numerical coefficient (for the second order moment,  $p=2$ , its theoretical value is  $G_1(2)=2$ ),  $\sigma$  is the standard deviation of the series,  $\Gamma(H)$  is gamma function

$$\Gamma(H) = \int_0^\infty e^t t^{H-1} dt. \quad (4.6)$$

$\Gamma(H, z)$  is the incomplete gamma function (the first one)

$$\Gamma(H, z) = \int_z^\infty e^t t^{H-1} dt, \quad (4.7)$$

$\gamma(H, z)$  is the incomplete gamma function (the second one)

$$\gamma(H, z) = \int_0^z e^t t^{H-1} dt = \Gamma(H) - \Gamma(H, z). \quad (4.8)$$

For small values of a difference moment lag, i.e.  $\Delta/L_1 = z=0$ , so

$$\gamma(H, z) = \int_0^z e^t t^{H-1} dt \approx z e^{z/2} (z/2)^{H-1}. \quad (4.9)$$

Then for the moment we have for  $\Delta \Rightarrow 0$ :

$$\Phi_{(p)}(\Delta) \propto \left(\frac{\Delta}{L_1}\right)^{H_p}. \quad (4.10)$$

The linear regression for the dependence  $\Phi_{(p)}(\Delta)$  in the double logarithmic axes, i.e. for the dependence  $\ln[\Phi_{(p)}(\Delta)]$  on  $\ln[\Delta]$ , for a small number of the first points (for example, three) gives the declination value  $H_p$ . Determining this declination and dividing it by the moment order  $p$ , we obtain the Hurst parameter  $H$ . Moments of the second order,  $p=2$ , were calculated. The parameters  $G_1$  and  $L_1$  were calculated by a special algorithm.

The specificity of ‘two-dimensional’ objects, such as surface patterns, is that they consist of a great number of series in two (as a minimum) independent directions. For the handling of such objects the following original procedure was developed (Vstovsky et al., 2001). A given (for example, 100) number of profiles in a given direction were randomly chosen in each pattern. Their parameterization was carried out by averaging their parameters in two ways. The first way was to calculate and parameterize the power spectrum and the difference moment for each chosen profile and then to calculate every necessary parameter as an average over the corresponding stored statistical collection. The second way was to calculate and average (over all the chosen profiles) the power spectrum and difference moment and then to calculate parameters for these averaged curves. The computed results for the parameters calculated in these two ways had insignificant differences, but the second way required considerably shorter calculation time. When the number of chosen profiles increased from 20 up to 100, the values of the parameters obtained varied by 2–5%. This value can be accepted as the estimation error of the obtained parameters.

All the calculations were carried out by means of a specially designed program FNSTV at identical ‘cuttings’ parameters of spectra and difference moments.

## Acknowledgements

This work was supported by the ISTC Grant No.2280.

## References

- Ben-David, T., Lereah, Y., Deutscher, G., et al., 1997. Correlated orientations in nanocrystal fluctuations. *Physical Review Letters* 78, 2585–2587.
- Collier, C., et al., 1999. Electronically configurable molecular based logic gates. *Science* 285, 391–394.
- Grafstrom, S., Kowalski, J., Neumann, R., 1990. Design and detailed analysis of a scanning tunneling microscope. *Measurement Science and Technology* 1, 139–146.
- Hiruma, T., Hamamatsu, K., 2002. Photonics. *Nature* 417, 521–526.
- Kunitake, M., Batina, N., Itaya, K., 1995. Self-organized porphyrin array on iodine-modified Au(111) in electrolyte solutions: in situ scanning tunneling microscopy study. *Langmuir* 7, 2337–2340.
- Labardi, M., Allegrini, M., Salerno, M., 1994. Dynamical friction coefficient map using a scanning force and friction force microscope. *Applied Physics* 59, 3–10.
- Lopinski, G., Wayner, D., Wolkow, R., 2000. Self-directed growth of molecular nanostructures on silicon. *Nature* 408, 48–51.
- Mitsui, T., Rose, M., Fomin, E., Ogletree, D., Salmeron, M., 2003. Dissociative hydrogen adsorption on palladium requires aggregates of three or more vacancies. *Nature* 422, 705–707.
- Neckers, D., 1967. Mechanistic Organic Photochemistry. NY Reinolds Publishing Corporation.
- Siegenthaler, H., 1992. 10 years of STM. In: Descouts, P., Siegenthaler, V. (Eds.), *Proceedings VI International Conference on Scanning Tunneling Microscopy*. Interlaken.
- Solovieva, A., Timashev, S., 2003. Catalyst systems based on immobilized porphyrins and metalloporphyrins. *Russian Chemical Reviews* 72, 965–984.
- Solovieva, A., Kotova, S., Timashev, S., et al., 2000. Deterministic quantum chaos in the system of vibration-rotation levels of porphyrin molecules according to IR spectroscopy data. *Russian Journal of Physical Chemistry* 74, 592–599.
- Solovieva, A., Kotova, S., Timashev, P., et al., 2003. The singlet oxygen generation photosensitized by deposited layers of tetraphenylporphyrin. *Russian Journal of Physical Chemistry* 1, 104–112.
- Srinivasan, R., Murphy, J., Fainchtein, R., 1991. Electrochemical STM of condensed guanine on graphite. *Journal of Electroanalytical Chemistry* 312, 293–300.
- Tao, N., Shi, Z., 1994. Monolayer guanine and adenine on graphite in NaCl solution: a comparative STM and AFM study. *Journal of Physical Chemistry* 98, 1464–1474.
- Timashev, S., 2000. Science of complexity: phenomenological basis and possibility of application to problems of chemical engineering. *Theoretical Foundations of Chemical Engineering* 34, 301–312.
- Timashev, S., 2001. Flicker-noise spectroscopy as a tool for analysis of fluctuations in physical systems. In: Bosman, G. (Ed.), *Proceedings XVI International Conference on Noise in Physical Systems and 1/f Fluctuations*. Gainesville.
- Timashev, S., Vstovsky, G., 2003. Flicker-noise spectroscopy in analysis of chaotic time series of dynamic variables and the problem of ‘signal-noise’ relation. *Russian Journal of Electrochemistry* 39, 156–169.
- Timashev, S., Vstovsky, G., Belyaev, V., 2003. Informative essence of chaos. In: Sikula, J. (Ed.), *Proceedings XVII International Conference on Noise in Physical Systems and 1/f Fluctuations*. Prague.
- Turro, N., Chow, M., Rigaudy, J., 1981. The mechanism of thermolysis of endoperoxides of aromatic compounds. Activation parameters, magnetic field and magnetic field effects. *Journal of American Chemical Society* 103, 7218–7224.
- Vstovsky, G., Solovieva, A., Kedrina, N., et al., 2001. Atomic force microscopy in analysis of the structure of composite materials. *Russian Journal of Physical Chemistry* 75, 1958–1963.
- Wada, Y., Tsukada, M., Fujihira, M., et al., 2000. Prospects and problems of single molecule information devices. *Japan Journal of Applied Physics* 39, 3825–3846.
- Yaminsky, I., Elensky, V.G., 1997. *Scanning Probe Microscopy*. Scientific World, Moscow.
- Yokoyama, T., Yokoyama, S., Kamikado, T., et al., 2001. Selective assembly on a surface of supramolecular aggregates with controlled size and shape. *Nature* 413, 619–622.
- Zambelli, T., Barth, J., Winterlin, J., et al., 1997. Complex pathways in chemisorption: O<sub>2</sub> on Pt(111). *Nature* 390, 495–497.